Journal of Inorganic and Organometallic Polymers and Materials (2020) 30:1726–1734
https://doi.org/10.1007/s10904-019-01284-z

Incorporation of Nanostructured ReO_3 in Silica Matrix and Their Activity Toward Photodegradation of Blue Methylene

C. Diaz[1] · M. L. Valenzuela[2] · O. Cifuentes-Vaca[3] · M. Segovia[1] · M. A. Laguna-Bercero[4]

Received: 12 July 2019 / Accepted: 14 August 2019 / Published online: 21 August 2019

Abstract

ReO_3 were prepared by thermal treatment of the macromolecular Chitosan·$(ReCl_3)_X$ and PSP-4-PVP·$(ReCl_3)_X$ precursors. The plasmon band in the visible region for the as obtained ReO_3 from their visible spectra was observed at λ_{max} of 640 nm. The nature of the polymeric precursor is acting as a solid state template and influences the size and morphology of the metal oxides. For the first time, the photocatalytic degradation of methylene blue using ReO_3 was measured founding a moderated and high activity for ReO_3 arise from Chitosan and PSP-4-PVP precursors respectively. The inclusion of ReO_3 into SiO_2 was performed using a combined solution of the Chitosan and PVP precursors by the sol–gel method. Subsequent pyrolysis of the solid precursors Chitosan·$(ReCl_3)_X(SiO_2)_y$ and PSP-4-PVP·$(ReCl_3)_X.(SiO_2)_y$ give rise to the nanocomposites ReO_3//SiO_2. The as obtained ReO_3 nanoparticles inside SiO_2 are small as 1 nm. The ReO_3 nanoparticles are distributed uniformly inside the matrix of SiO_2, leading to stable semi porous materials suitable for high temperature catalytic application. The composites ReO_3/SiO_2 exhibit a moderate photocatalytic activity toward the degradation of methylene blue and similar to that of ReO_3.

Graphic Abstract

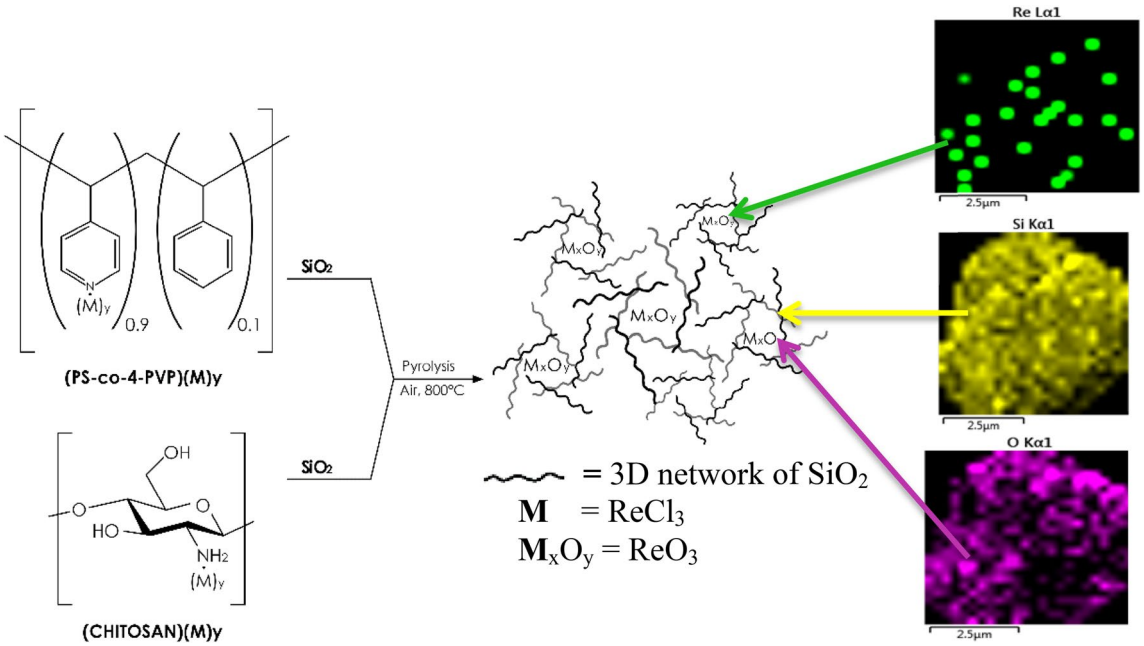

Electronic supplementary material The online version of this article (https://doi.org/10.1007/s10904-019-01284-z) contains supplementary material, which is available to authorized users.

Extended author information available on the last page of the article

Keywords Nanostructured ReO3 · Photodegradation · Blue methylene

1 Introduction

Rhenium differ considerably from manganese, despite similarities in the stoichiometry of a few compounds (e.g. the series MnO_4^-, TcO_4^-, ReO_4^-). Re has little cationic chemistry but they have extensive chemistry in the IV, V and VI state [1]. Among rhenium oxides, ReO_3 exhibit some catalytic activity in organic reactions. Their activity is hugely enhanced at the nano-level [2, 3]. The most interesting property of ReO_3 is their metallic behavior with conductivity closes that of copper [4–6].

Although isolated solution preparation methods for ReO_3 [4–9] is well documented, no solid-state general ways to prepare these nanostructured metal oxides have been reported. Re, metal oxides have been obtained by solvothermal treatment of the precursors $Re_2O_7{\cdot}C_4H_8O_2$ at 200 °C [5]. ReO_3 nanowires have been prepared via a simple vapor transport at 300 °C [7] and their SERS activity toward aza-aromatic compounds has been measured [6]. The photodegradation activity of methyl orange using ReO_3 has been measured found a high catalytic efficiency.

Here we report a general and suitable method for the preparation of Re metal oxides nanostructured materials [10–12]. Regarding to the possible application of these Re metal oxides, the first step is usually their incorporation in solid matrices. Additionally, when the application of these nanostructured metal oxides involves high temperatures, the metal oxide inside the matrix must be stable [13, 14]. The incorporation of metal-oxide nanoparticles into solid devices is not straightforward [13, 14] when they are produced via a solution phase method because the solid-state isolation of the nanoparticles usually causes nanoparticle agglomeration [15–18]. Thus, the incorporation of metal-oxide a nanoparticle generated directly from a solid-state approach appears to be the most reliable method.

A general method to prepare Re nanostructured metal oxides is shown in Scheme 1. Stable nanocomposites// SiO_2 are obtained by a high temperature thermal treatment of the precursors Chitosan·$(ReCl_3)_n$//SiO_2 and PS-co-4-PVP·$(ReCl_3)_n$//SiO_2,as seen in Scheme 2.

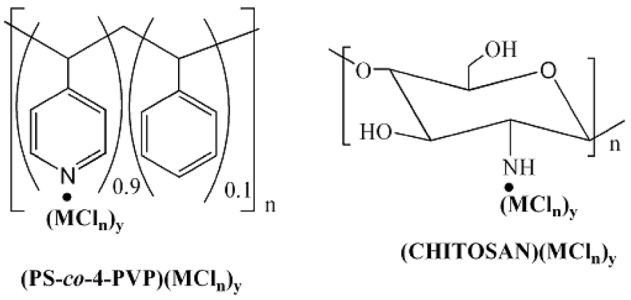

Scheme 1 General representation of complexes of polymer-metal structure

2 Experimental

Preparation of complexes of polymer-metal: In 20 ml dichloromethane, a stoichiometric amount of the polymer (1:1 polymer:complex) and 0.40 g of metal complexes was

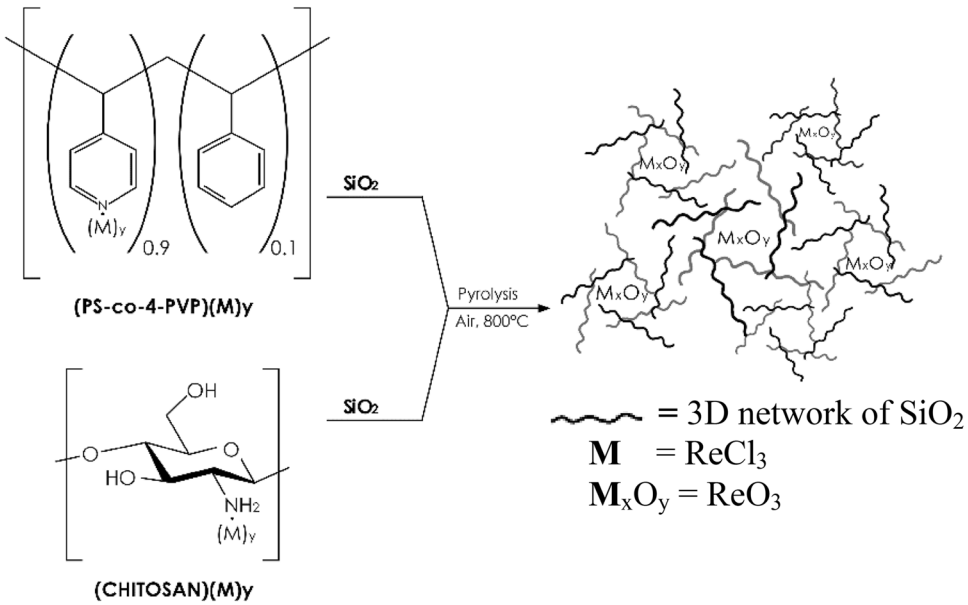

Scheme 2 General representation of the inclusion of the Re nanostructured metal oxide into SiO_2

added. The heterogeneous mixture was stirred at room temperature for 8 days. The as obtained solid was washed with dichloromethane and dried under vacuum during 3 h. Details are given in Table S1 of Supplementary Materials.

Pyrolysis: The complexes of polymer-metal were placed into a box furnace (lab tech) using a temperature program of pyrolysis at 180 °C.

Preparation of complexes of polymer-metal//Silica: In 20 ml dichloromethane, a stoichiometric amount of the polymer (1:1 polymer: complex) and 0.40 g of metal complexes was added. The heterogeneous mixture was stirred a room temperature for 8 days and then silica sols were added. This was prepared by mixing TEOS, acetic acid and H_2O mili-Q (1:4:4 TEOS: Acetic Acid: H_2O) at room temperature under stirring for 5 h. The resulting gel was dried in a vacuum-oven at 80 °C and then calcined at 800 °C, except for Re which was calcined at 180 °C. The summary of the as obtained products is given in Table 1.

Characterization: X-ray diffraction (XRD) was conducted at room temperature on a Siemens D-5000 diffractometer with θ-2θ geometry. XRD data was collected using Cu-*K*α radiation (40 kV, 30 mA). Elemental microanalysis was performed by energy dispersive X-ray analysis using a NORAN Instrument micro-probe attached to the scanning electron microscopy. SEM images were acquired with a Philips EM 300 scanning electron microscope. Energy dispersive X-ray analysis (EDAX) was performed on a NORAN Instrument micro-probe attached to a JEOL 5410 scanning electron microscope. High-resolution transmission electron microscopy (HR-TEM) was performed using a JEOL 2000FX TEM microscope at 200 kV to characterize the average particle size, distribution and elemental and crystal composition. The average particle size was calculated using the Digital Micrograph software. Methylene Blue (MB) was used as a model compound to test the photocatalytic properties at 655 nm under UV–Vis illumination using a xenon lamp (150 W) positioned 20 cm away from the photoreactor in a range 330–680 nm at room temperature, to avoid the self-degradation and thermal catalytic effects of cationic dye MB.

Table 1 Yields, color and composition of the pyrolytic products from the respective precursors

Precursor polymer	Formula	Yield (%)	Color	Composition
(1)	PS-co-4-PVP·$(ReCl_3)_n$	47	Black	$ReCl_3/ReO_3$
(2)	Chitosan·$(ReCl_3)_n$	56	Black	$ReCl_3/ReO_3$
(3)	PS-co-4-PVP·$(ReCl_3)_n$//SiO_2	99	Grey	ReO_3/SiO_2
(4)	Chitosan·$(ReCl_3)_n$//SiO_2	64	Grey	ReO_3/SiO_2

3 Results and Discussion

The Chitosan·$(ReCl_3)_X$ and PSP-4-PVP·$(ReCl_3)_X$ precursors were characterized by TG/DTA analysis. The presence and the degree coordination of the $ReCl_3$ to both polymer backbone were performed by TG analysis under air. The pyrolytic residue corresponds to ReO_3 in both cases and by mass difference and comparing with the macromolecular complex with a 100% coordination the degree coordination can be estimated. Values are similar near at 80%. Thus the TG analysis confirm the presence of both Chitosan and PS-co-4-PVP slightly modified by coordination of the $ReCl_3$, see Electronic Supplementary Materials S2.

For the Chitosan·$(ReCl_3)_X$ for instance the weight loss at 1883 °C can be assigned to the decomposition (carbonization) of the NH_2, CH_2OH and OH groups side to the main carbon ring of the Chitosan. On the other hand the weight loss at 360 °C can be assigned to the decomposition of the skeleton carbon of the Chitosan both weight loss modified to lesser temperatures than free Chitosan due to the coordination to the polymer decrease the thermal stability as is usually observed. These two main weight loss are accompanied of exothermal processes a observed by the respective exothermal peaks in the ATG curve at temperatures 221 °C and around 540 °C.

XRD patterns of the as prepared ReO_3 from precursor both with Chitosan as solid state template are shown in Fig. 1. For the PSP-4-PVP precursor similar XRD patern was found (not showed). For both templates, ReO_3 phase was obtained, in concordance with different preparation

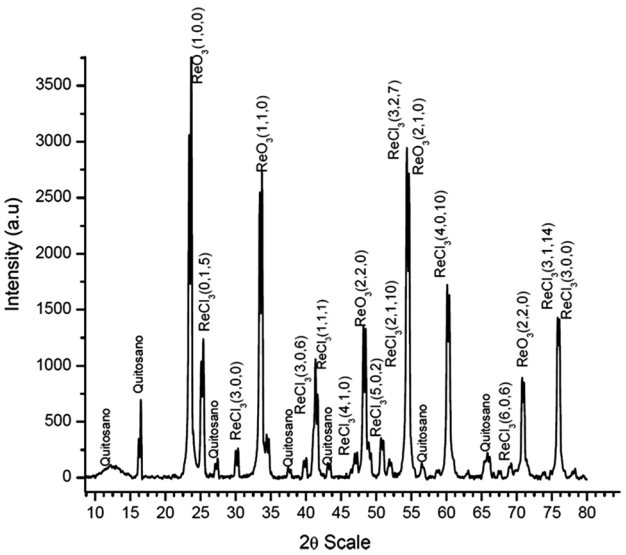

Fig. 1 XRD pattern of SEM image of ReO_3 from the precursor Chitosan·$(ReCl_3)_X$

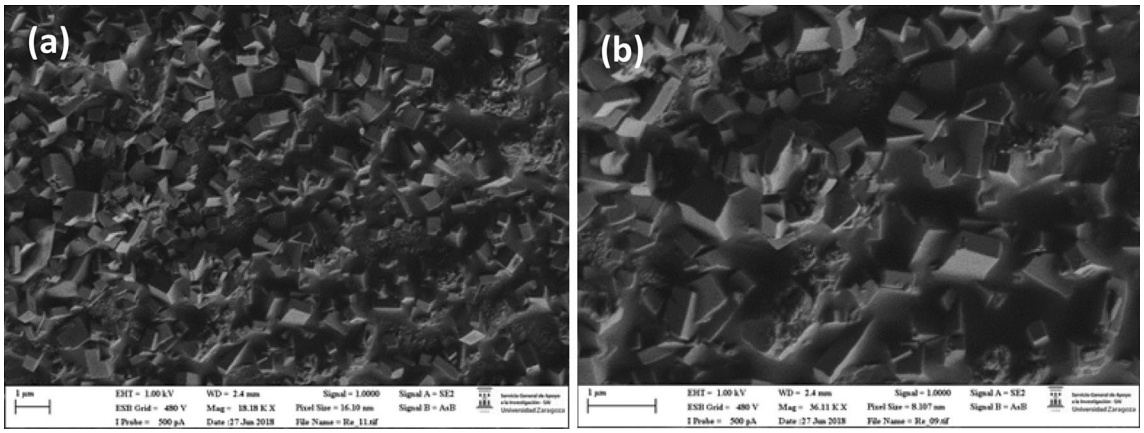

Fig. 2 SEM image of ReO_3 (**a**, **b**)

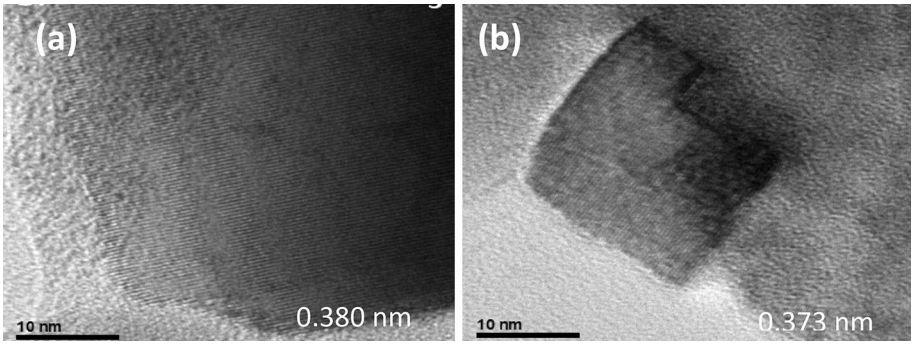

Fig. 3 HRTEM of ReO_3 obtained from Chitosan (**a**, **b**)

methods [5–8]. However some impurities of $ReCl_3$, in addition to rhenium oxide [4–6] were observed, see Fig. 1.

SEM analysis for the pyrolytic product from PSP-4-PVP·$(ReCl_3)_X$ shows a cuboid with a distorted ReO_3 [19] in Fig. 2.

HR-TEM for the ReO_3 sample obtained from the Chitosan precursor (see Fig. 3) also shows typical particle sizes in the range of 10–20 nm. Similar well defined HRTEM images have been reported for ReO_3 obtained using a reduction method from the Re_2O_7 precursor [19].

Due to the well-known conductor behavior [5] nanostructured ReO_3 exhibits a plasmon band in the visible region [5]. For ReO_3 from their visible spectra (see Electronic Supplementary S3) a λ_{max} of 640 nm was observed shifted to most large wavelengths due to a sum most bigger size respect to those reported by Rao [5].

If the preparation methods (all in solution) for ReO_3 oxides are scarce [4–9], more limited are those for the oxides into SiO_2, being the only one the core/shell ReO_3/SiO_2 structures reported by Ghosh et al. [8]. In this work we propose the incorporation of ReO_3 into sol–gel SiO_2 by using the respective macromolecular precursors Chitosan·$(ReCl_3)_X$ and PSP-4-PVP·$(ReCl_3)_X$. The phase purity of the ReO_3//SiO_2 products was characterized by X-ray diffraction.

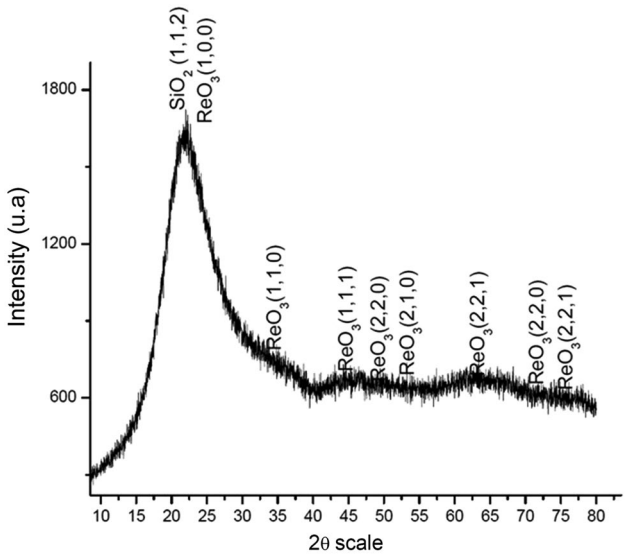

Fig. 4 XRD of ReO_3//SiO_2 from Chitosan·$(ReCl_3)_X$//SiO_2

Finally, XRDs for ReO_3//SiO_2 nanocomposites produced from chitosan is shown in Fig. 4. The broad peak around $2\theta = 15°–25°$ observed in all these nanocomposites is typical of amorphous SiO_2 as matrix in metal

oxide nanostructured inside [10–22]. Unfortunately, the diffraction peaks of ReO_3 are not clearly observed probably due to their small size, as it will be later confirmed by HR-TEM. The XRD for ReO_3//$SiO_2$from the polymer PVP exhibits a similar XRD corroborating also the similar phase for ReO_3//SiO_2 (not showed).

From the HR-TEM image of the nanocomposite ReO_3// SiO_2 using the PVP precursor, small nanoparticles (~ 1 nm) of ReO_3 included in SiO_2 matrix can be observed, as shown in Fig. 5a–d. This can be due to the small confinement of the ReO_3 nanoparticles imposed by the SiO_2 network. It is also worth noting that the Chitosan precursor helps to enhance de distribution of ReO_3 particles along the SiO_2 matrix, as it was more difficult to find the nanoparticles on the sample obtained from the PVP precursor.

Additional information about the uniform distribution of the ReO_3 nanoparticles inside silica was obtained by EDX mapping from SEM images, as shown in Fig. 6 for ReO_3// SiO_2 obtained for both precursors.

3.1 Photocatalytic Behavior ReO_3

Methylene blue is one of the organic dyes which are extensively used in coloring paper, temporary hair colorant, dyeing cotton and coating for paper stock [23].We use this dye as model dye to assay the photocatalytic properties of ReO_3.The removal of this hazardous dye is considered as one of the growing needs in recent years. The photocatalytic experiments were carried on the catalyst ReO_3 samples with definite concentrations under dark conditions

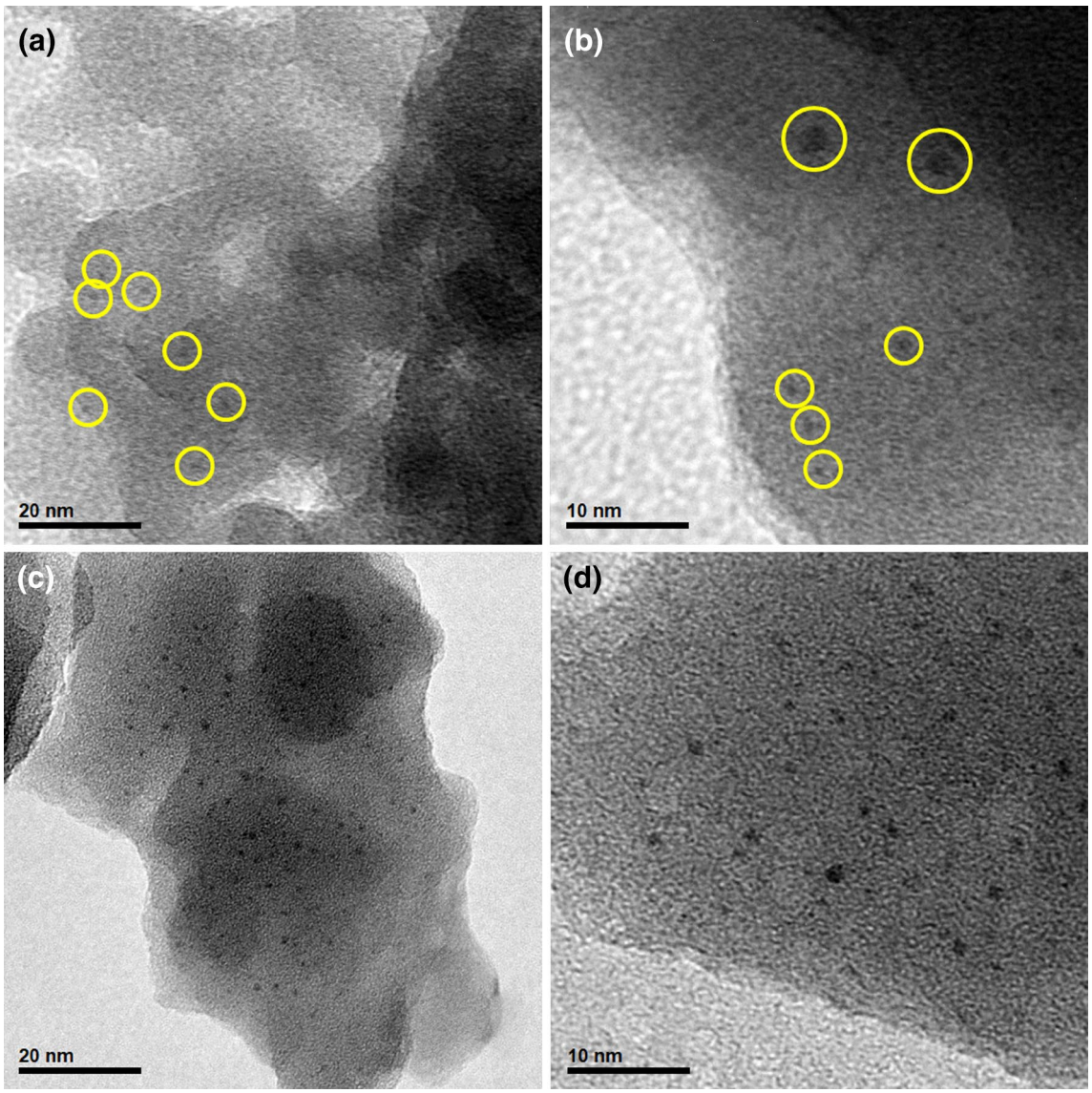

Fig. 5 HRTEM images of ReO_3//SiO_2 obtained from the PVP (**a**, **b**) and chitosan precursors (**c**, **d**)

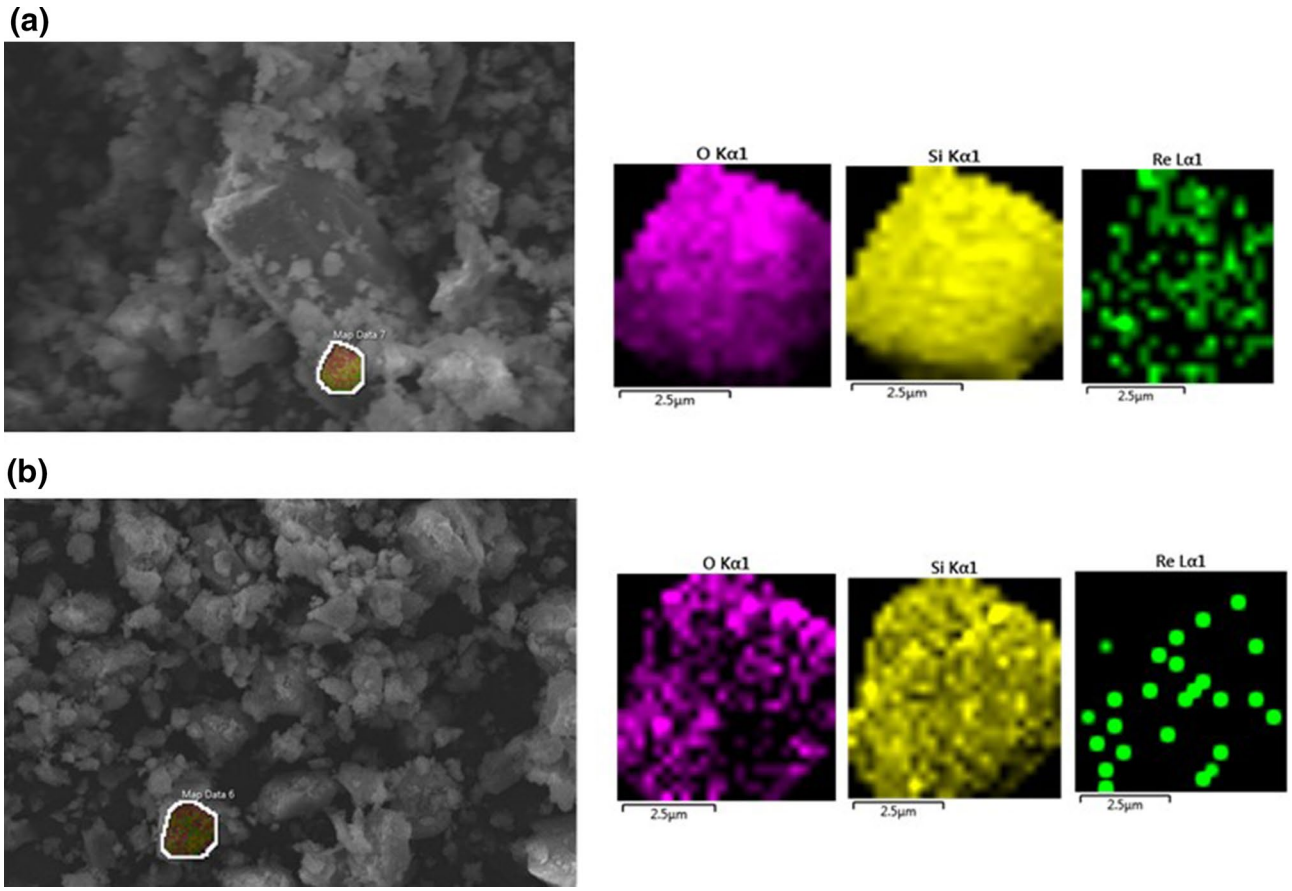

Fig. 6 EDX-elemental mapping of ReO_3 nanoparticles inside silica from precursor (Chitosan·$(ReCl_3)_X$//SiO_2 (**a**) and from precursor PSP-4-PVP·$(ReCl_3)_X$//SiO_2 (**b**)

and with UV irradiations in attempts to prove their efficiency. Methylene blue (MB) was used a model dye to test the photocatalytic behavior of the nanostructured ReO_3. In Electronic Supplementary Materials S4 are showed the absorption spectra vs time of the different oxides.

In addition, ReO_3 was also found to catalyze the photodegradation of MB with an efficiency of 53% and 64% in 300 min, for the chitosan and PVP precursors, respectively. ReO_3 is an unusual transition metal oxide, as it presents a metallic behavior with conductivity close to that of copper [5]. Thus nanoparticles of rhenium trioxide produce SERS (surface-enhanced Raman spectra) effect for some organic compounds as pyridine [6]. In spite of this, their catalytic activity has been only proved in catalytic degradation of methyl orange [9]. Figure 7a shows the plot of C/C_o versus irradiation time for ReO_3 obtained from Chitosan as well as from PVP precursors, being the degradation capacity very similar for both samples. As shown in Fig. 7b, the kinetic of the degradation follow a first order processes for ReO_3 obtained both from Chitosan as well as from PVP precursors.

3.2 Photocatalytic Behavior of ReO_3/SiO_2 Composites

With the purpose to compare the photocatalytic efficiency of ReO_3 with their composite ReO_3/SiO_2 the photodegradation of blue methylene was performed. Although the composite ReO_3/SiO_2 was reported by Rao [8] their photocatalytic activity has been not investigated with blue methylene neither with another dye contaminant. Figure 8 shows the degradation curve of methylene blue with the composite ReO_3/SiO_2 from the PSP-co-4-PVP and from the Chitosan polymer precursors. From these curves degradation about 67% and 57% of degradation in 330 min were found. The degradation kinetic for both composites follow a first order for the composite from PSP-co-4-PVP while that for the Chitosan precursor polymer follow a zero order see Electronic Supporting Material S5. These values are similar to the photocatalytic activity of photocatalytic activity of ReO_3 without their incorporation inside silica. On the other hand, in Fig. S6 of Supporting Material are showed the absorption spectra vs time of the different oxides.

Table 2 summarizes the kinetic data for the degradation of MB with ReO_3/SiO_2-PS-4-PVP and ReO_3/SiO_2-Chitosan. Due to their no literature report for photodegradation of MB with the ReO_3 and ReO_3/SiO_2 materials the comparison is not possible. However, some comparison within them can be made. The higher photocatalytic efficient the composite ReO_3/SiO_2-PS-4-PVP is in agree with the higher rate constant. With regarding the effect of the SiO_2 matrix on the

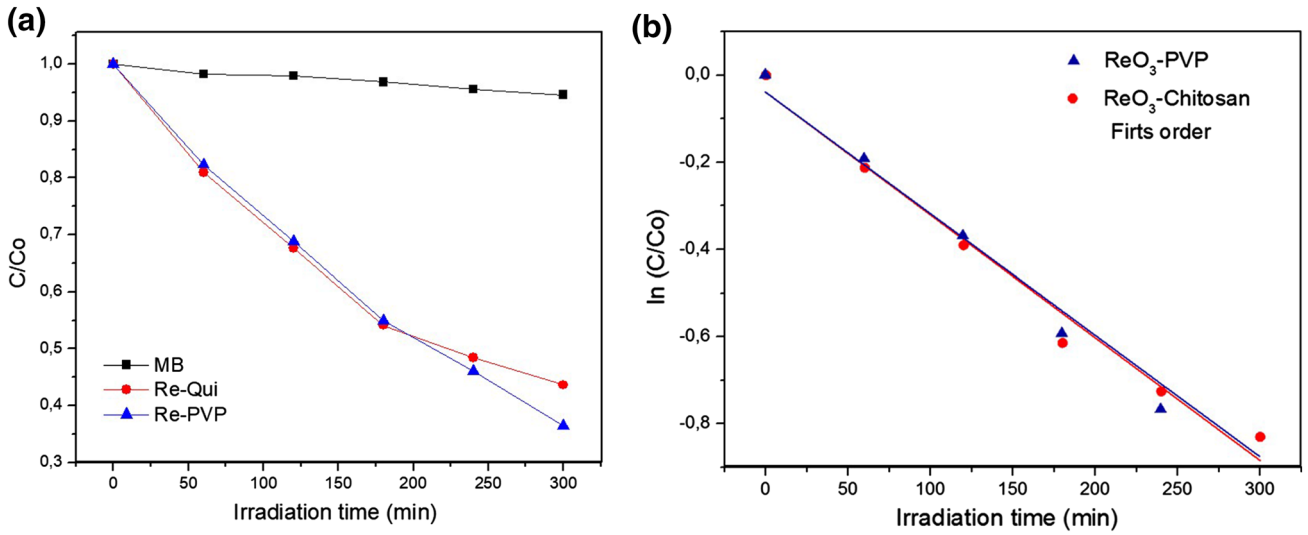

Fig. 7 **a** Normalized concentration changing of MB without catalyst, in presence of ReO_3-PVP and in presence of ReO_3-Chitosan. **b** Normalized concentration changing of MB (ln C/Co) vs time for the ReO_3-Chitosan precursor

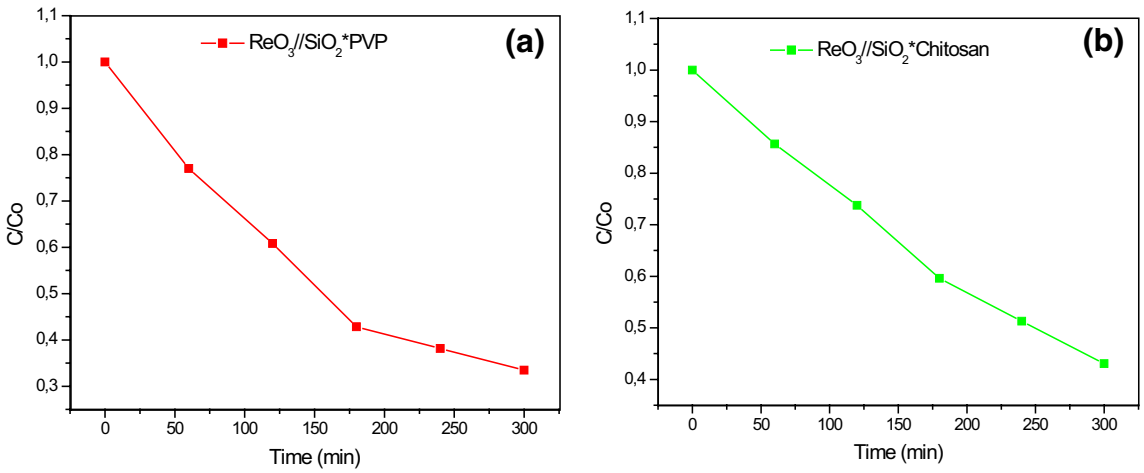

Fig. 8 Normalized concentration changing of MB without catalyst, in presence of ReO_3/SiO_2-PVP (**a**) and in presence of ReO_3/SiO_2-Chitosan (**b**)

Table 2 Kinetic data for the photodegradation process of MB with ReO_3 and ReO_3/SiO_2

Photocatalyst	Photodegradation rate constant k (10^{-3}M·min^{-1})	Discoloration rate (%)	R^2 linear fit (%)
ReO_3-PS-4-PVP	2.8	64	0.977
ReO_3-Chitosan	2.8	53	0.977
ReO_3/SiO_2-PS-4-PVP	3.7	67	0.978
ReO_3/SiO_2-Chitosan	1.9	57	0.985

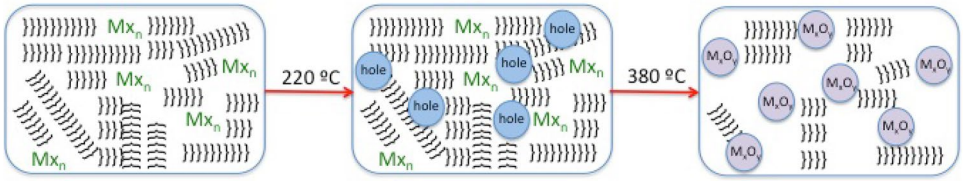

Fig. 9 Schematic representation of the proposed mechanism of formation of the metal oxide nanoparticles. MX_n represent the general formula of the metallic salt coordinated to the Chitosan polymer and }}}}}}} represent the polymeric Chitosan. The temperature are referential general values

photocatalytic efficient measured in degradation percentage, the composite ReO_3/SiO_2-PS-4-PVP material increases slightly their photocatalytic efficient. Thus, from Table 2, the discoloration rate is in agreement with the photodegradation rate for all the materials.

3.3 Probable Formation Mechanism

Some insight about the formation mechanism of the nanostructured Re metal oxides materials from both precursors can be proposed using the mechanism of formation of nanostructured metallic materials from the oligomer precursor $\{NP(OC_8H_{12})_2(OC_6H_4PPh_2\text{-}Mn(CO)_2(\eta^5\text{-}C_5H_4Me)_2\}_n$ [24]. A schematic representation of this process is provided in Fig. 9. Briefly the first step on heating involves the formation of a 3D network to produce a thermally stable matrix. This step is crucial because it offsets the sublimation. The first heating step could involve a cross linking of the Chitosan or PSP-4-PVP polymer giving a 3D matrix containing the $ReCl_3$ compound linked to the polymeric chain. The following steps could involve the starting of the organic carbonization, producing holes where the nanoparticles begin to nucleate. As it was confirmed in earlier studies [10, 24], the ReO_3 oxide grow over layered graphitic carbon host which is lost near to the final annealing temperature i.e. 800 °C.

4 Conclusions

A general solvent less method using the easily synthetized precursors Chitosan·$(ReCl_3)_X$ and PSP-4-PVP·$(ReCl_3)_X$ affords the nucleation ReO_3 metal oxides. Incorporation of these metal oxides into SiO_2 matrix was achieved using a thermal treatment of the chitosan and PVP precursors to give the $ReO_3//SiO_2$ composites. Some $ReCl_3$ present in the ReO_3 was absent in the $ReO_3//SiO_2$ composite. A regular distribution of the respective nanoparticles inside SiO_2 was observed. For the $ReO_3//SiO_2$ sample, ReO_3 nanoparticles of about 1 nm were obtained. Photocatalytic degradation of MB using ReO_3 was measured for the first time, founding a high activity. The photocatalytic activity of ReO_3 increase when their incorporation inside SiO_2.

Acknowledgements The authors acknowledge Fondecyt Projects 1160241 for financial support. This research has also received funding from Consejo Superior de Investigaciones Científicas, Spain under grant I-COOP LIGHT 2015CD0013. The use of Servicio General de Apoyo a las Investigación (SAI, University of Zaragoza) is also acknowledged.

References

1. F.A. Cotton, G. Wilkinson, *Advanced Inorganic Chemistry, Chapters 22 and 30* (Wiley, New York, 1980), p. 1980
2. R. Jin, Nanotechnol. Rev. **1**, 31–56 (2012)
3. M. Fernandez-Garcia, A. Martinez-Arias, J. Hanson, C. Rodriguez, Chem. Rev. **104**, 4063–4104 (2014)
4. K. Biswas, C.N. Rao, J. Nanosci. Nanotechnol. **7**, 1969–1974 (2007)
5. K. Biswas, C.N. Rao, J. Phys. Chem. B **110**, 842–845 (2006)
6. K. Biswas, C.N. Rao, J. Phys. Chem. C **111**, 5689–5693 (2006)
7. D. Myung, Y. Lee, J. Lee, H. Yu, J. Lee, J. Baik, W. Kim, M. Kim, Phys. Status Solid (RRL) **4**, 365–367 (2010)
8. S. Ghost, K. Biswas, C.N. Rao, J. Mater. Chem. **17**, 2412–2417 (2007)
9. Y. Chong, W. Fan, J. Colloid Interface Sci. **397**, 18–23 (2013)
10. C. Díaz, M.L. Valenzuela, M.A. Laguna-Bercero, A. Orera, D. Bobadilla, S. Abarca, O. Peña, RSC Adv. **7**, 27729–27736 (2017)
11. C. Díaz, M.L. Valenzuela, M. Segovia, R. de la Campa, A. Presa, J. Clust. Sci. **29**, 251–266 (2018)
12. C. Diaz, O. Crespo, C. O'Dwyer, C. Gimeno, A. Laguna, I. Ospino, M.L. Valenzuela, Inorg. Chem. **54**, 7260–7269 (2014)
13. B. Teo, X. Sun, Chem. Rev. **107**, 1454–1532 (2007)
14. G.B. Khomutov, V.V. Kislov, M.N. Antipirina, R.V. Gainutdinov, S.P. Gubin, A. Obydenov, S.A. Pavlov, A.A. Rakhnyanskaya, A.N. Sergeev-Cherenkov, E.S. Soldatov, D.B. Suyatin, A.L. Toltikhina, A. Trifonov, T.V. Yurova, Microelectron. Eng. **69**, 373–383 (2003)
15. M.P. Pileni, Acc. Chem. Res. **40**, 685–693 (2007)
16. M.P. Pileni, J. Mater. Chem. **21**, 16748–16758 (2001)
17. Y.F. Wan, N. Goubet, P.A. Albouy, M.P. Pileni, Langmuir **29**, 7456–7463 (2013)
18. C. Díaz, M.L. Valenzuela, in *Valenzuela in Encyclopedia of Nanoscience and Nanotechnology*, vol. 16, ed. by H.S. Nalwa (American Scientific Publishers, Valencia, 2010), pp. 239–256
19. L.C. Kozy, M.N. Tahir, C. Lind, W. Tremel, J. Mater. Chem. **19**, 276–2765 (2009)
20. Y. Li, Y. Hu, H. Jiang, Ch. Li, Nanoscale **5**, 5360–5367 (2013)
21. Y. Kuwahara, N. Furuichi, H. Seki, H. Yamashit, J. Mater. Chem. A **5**, 18518–18526 (2017)
22. C. Wang, J. Li, X. Liang, Y. Zhang, G. Guo, Energy Environ. Sci. **7**, 2831–2867 (2014)

23. M. Tamura, K. Tokonami, Y. Nakagawa, K. Tomishige, ACS Sustain. Chem. Eng. **5**, 3685–3697 (2017)
24. C. Díaz, M.L. Valenzuela, V. Lavayen, C. O'Dwyer, Inorg. Chem. **51**, 6228–6236 (2012)

Affiliations

C. Diaz[1] · M. L. Valenzuela[2] · O. Cifuentes-Vaca[3] · M. Segovia[1] · M. A. Laguna-Bercero[4]

✉ M. L. Valenzuela
maria.valenzuela@uautonoma.cl

[1] Departamento de Química, Facultad de Química, Universidad de Chile, La Palmeras 3425, Nuñoa, casilla 653, Santiago de Chile, Chile

[2] Universidad Autónoma de Chile, Instituto de Ciencias Químicas Aplicadas, Facultad de Ingeniería, Inorganic Chemistry and Molecular Material Center, Av. El Llano Subercaseaux 2801, San Miguel, Santiago de Chile, Chile

[3] Facultad de Ciencias Exactas, Universidad Andrés Bello, Sede Concepción, Autopista Concepción-Talcahuano 7100, Talcahuano, Chile

[4] Instituto de Ciencia de Materiales de Aragón (ICMA), CSIC- Universidad de Zaragoza, C/Pedro Cerbuna 12, 50009 Zaragoza, Spain